ARTICLE

Ultrafast Spectroscopic Investigation on Fluorescent Carbon Nanodots: the Role of Passivation

Received 00th January 20xx,
Accepted 00th January 20xx

DOI: 10.1039/x0xx00000x

Alice Sciortino,[a, b, c] Michela Gazzetto,[c] Maria Laura Soriano,[d,e]* Marco Cannas,[a] Soledad Cárdenas,[d] Andrea Cannizzo[c]*and Fabrizio Messina[a,f]*

Disentangling the respective roles of the surface and core structures in the photocycle of Carbon Nanodots is a critical open problem in carbon nanoscience. While the need of passivating Carbon dot surfaces to obtain efficiently emitting nanoparticles is very well-known in the literature, it is unclear if passivation introduces entirely new surface emitting states, or if it stabilizes existing states making them fluorescent. In this multi-technique femtosecond spectroscopy study, the relaxation dynamics of non-luminescent (non-passivated) carbon dots are directly compared with their luminescent (passivated) counterparts. Non-passivated dots are found to host emissive states, albeit very short-lived and practically incapable of steady-state fluorescence. In contrast, the passivation procedure gives birth to a distinctive new manifold of emitting states, localized on the surface of the dots, and capable of intense, tunable, long-lived fluorescence. It turns out that these surface states are instantaneously populated by photo-excitation, and their subsequent dynamics are entirely independent of core electronic transitions. The experiments reveal the lack of any crosstalk between core- and surface states, at least for certain common types of carbon dots, and open a new perspective on the mechanisms by which surface passivation governs the fluorescence properties of these nanoparticles.

Introduction

Carbon nanodots are now recognized as an emerging family of nanomaterials which display various interesting optical properties. In particular, they are well-known for their tunable fluorescence, whose emission quantum yield can be very high (50-70 %),[1–4] although the spectral characteristics and actual brightness are, in practice, highly synthesis dependent. In the literature, they are sometimes described as carbon "quantum" dots (CQDs), at least when they display well-defined nanocrystalline core structures. [5] However, the actual role of "quantum" effects in the electronic properties of CQDs is very disputed. [6,7] In particular, it is not clear yet if their fluorescence originates from electronic transitions within the carbonaceous core of the nanoparticles, [8] from the radiative recombination of charge carriers localized on the surface, [1,9] or if it is related to small, independent molecular fluorophores linked to the dots. [10,11] Even assuming a key role of emissive surface states, it is unclear if their excitation occurs by a direct or indirect mechanism. In regard to the latter, the core-surface electronic coupling is being more and more highlighted by recent work.[12] On one hand, several authors have proposed that photons absorption initially involves electronic transitions localized in the carbonaceous core which, only later, transfer the excitation onto surface states. [13-16] In contrast, other works have proposed that both the absorption and the emission transitions directly occur on surface defects. [1,17,18] Overall, elucidating the interplay between core and surface states in controlling CQD optical transitions stands as one of the key open problems in the field. Moreover, to further complicate the fundamental understanding of the fluorescence mechanism, the emission properties of CQDs are strongly dependent on several synthesis parameters, as the precursors, [19] synthesis temperature, [20] and surface modifications. [21]

Surface modifications are important for several different nanomaterials, as a direct consequence of the very large surface area-to-volume ratio[22]. Because of the small size, the latter can reach extremely high values even for non-porous

[a]*Dipartimento di Fisica e Chimica - Emilio Segrè, Universitá degli Studi di Palermo, Via Archirafi 36, 90123 Palermo, Italy. E-mail: fabrizio.messina@unipa.it*
[b]*Dipartimento di Fisica e Astronomia, Universitá degli Studi di Catania, Via Santa Sofia 64, 95123 Catania, Italy.*
[c]*Institute of Applied Physics, University of Bern, Sidlerstrasse 5, CH-3012 Bern, Switzerland.*
E-mail: andrea.cannizzo@iap.unibe.ch
[d]*Department of Analytical Chemistry, Institute of Fine Chemistry and Nanochemistry, Marie Curie Annex Building. Campus de Rabanales, 14071 Córdoba, Spain. E-mail: laura.soriano@uclm.es*
[e]*Regional Institute for Applied Chemistry Research (IRICA), 13004 Ciudad Real, Spain.*
[f] *CHAB - ATeN Center, Universitá degli Studi di Palermo, Viale delle Scienze, Edificio 18, 90128 Palermo, Italy.*
Electronic Supplementary Information (ESI) available: Additional femtosecond pump/probe and fluorescence upconversion spectra and comparisons. See DOI: 10.1039/x0xx00000x

nanomaterials. Indeed, the surface (type and density of functional groups) and its treatments are usually essential to achieve colloidal stability of the nanoparticles in solution.[23] Moreover, in the case of CQDs, several works demonstrated that the passivation of the surface is fundamental to activate an intense emission, [24] although it is unknown if passivation introduces new surface emitting states or if it stabilizes existing states making them fluorescent. It is well known that raw CQDs (r-CQDs) produced by top-down methods are usually non-emissive,[25,26] and some works demonstrated that the fluorescence characteristics depend on the density of surface functional groups,[21,27] confirming that the emission involves surface electronic transitions. However, in a recent work we showed that passivating CQD surfaces by various different functional groups surprisingly produces a spectrally identical emission. [28] On these grounds, it was suggested that the fluorescence is related to very delocalized surface electronic states which spread over a large portion of the surface shell. Thus, these emissive states cannot be uniquely traced back to any specific functional group, not even in principle.

To shed light on these questions, and particularly on the role of passivation and core-to-surface interplay in governing CQD fluorescence, we used ultrafast spectroscopic methods to thoroughly investigate the photocycle of graphitic CQDs synthesized by a top-down approach using multi-walled carbon nanotubes as precursors. The strategy of our experiment is to compare the properties of non-emissive r-CQDs to their strongly emissive, carboxyl-passivated counterparts (p-CQDs), with the goal of determining the mechanism by which this surface passivation activates the emission. In this respect, it is worth noting that the photocycle of r-CQDs cannot be studied by traditional, continuous-wave optical spectroscopies, because of a lack of steady-state emission. Therefore, a thorough comparison between the optical responses of r- and p-CQDs has been impossible so far. However, the lack of emission in r-CQDs suggests an extremely fast non-radiative depopulation of the excited state, which should not be a limitation for femtosecond optical methods. Therefore, femtosecond spectroscopy can be used to open an observable window on r-CQDs, and directly compare them to p-CQDs. Through this approach, we show that surface passivation makes CQDs emissive by introducing an entirely new manifold of emissive states on the surface, which are characterized by a continuum of different energies. Besides, we demonstrate that core-to-surface excitation transfer can be ruled out: emissive surface states are directly populated by photo-excitation, and are completely independent of core states. Noteworthy, we also show that even the non-passivated dots host emissive states, although they decay in a very short time hindering any practical long-lived emission. Finally, thanks to these very fast decays, r-CQDs also allow to isolate a transient spectroscopic observable deriving from core states, which would usually be hidden under surface states signatures.

Experimental Section

Synthesis

Graphitic CQDs have been synthesized by a top-down methodology explained in details in ref. 29 and here briefly. 200 mg of multi-walled carbon nanotubes (MWCNTs) in 20 mL of a solution containing 3:1 H_2SO_4/HNO_3 were refluxed at 140°C for 7.5 h. At this point the raw non-luminescent sample is ready, referred to as raw-CQDs (r-CQDs). After cooling down to room temperature, 40 mL of acetone were added and a dark brownish solution was left to stand overnight. Such a treatment with acetone allows passivation with C=O moieties of the surface of nanoparticles formed through the chemical oxidation of MWCNTs. The passivated CQDs (here named p-CQDs) are luminescent. The nanoparticles were then neutralized and centrifuged at 13000 rpm for 10 min to remove large aggregates. Afterward, excess of salts were removed with ethanol by crystallization at low temperatures.

Steady State Absorption

Optical absorption spectra of CQDs in aqueous solution were recorded on a JASCO V-560 double-beam spectrophotometer in 1 cm optical length quartz cuvettes at room temperature. The measurements were performed at room temperature.

Steady State Emission

The emission spectra were recorded on diluted aqueous solutions (0.005 g/L) with a JASCO FP-6500 spectrofluorometer in a 1 cm cuvette with a 3 nm resolution bandwidth. The measurements have been performed at room temperature.

Infrared Absorption

IR spectra were performed on KBr pellets containing the CQDs with a FT-MIR Tensor 27 spectrophotometer equipped with a microscope Hypeion 2000. All analyses were carried out at room temperature.

Fluorescence Upconversion

Femtosecond fluorescence upconversion (FlUC) measurements were carried out in a home-built setup described hereafter. The laser source is a 5 kHz Ti:sapphire femtosecond amplifier with an output beam spectrally centered at 800 nm (50 fs pulse with 350 μJ energy/pulse). The beam is used to generate the excitation beam at 400 nm by frequency doubling within an ultrathin (250 μm) β–barium borate (BBO) crystal. After removing the residual of the fundamental beam at 800 nm with a BG40 filter, the 400 nm beam is chopped (500 Hz), and then focused on the sample (continuously flowing into a 200 μm thick cell) by a parabolic mirror with a focal length of 50 mm. After excitation of the sample, the spontaneous emission is collected and collimated by second parabolic mirror with focal length of 50 mm and a diameter of two inches and directed to a third parabolic mirror with the same diameter and a focal length of 250 mm, which

focuses the fluorescence into a 250 µm thick sum-frequency BBO crystal, where the fluorescence finally overlaps with the delayed "gate" beam. The gate beam (800 nm) is focused on the same crystal with a lens having a focal length of 1 m. In these conditions, the sizes of the two spots on the crystal are about 250 and 350 µm, respectively. The angle between the gate and the fluorescence is usually 4°. Sum-frequency generation between fluorescence and gate generates an UV beam, the intensity of which is proportional to that of the fluorescence, which is detected after the sum-frequency BBO.

The upconverted emission generated within the non-linear crystal passes through a dispersive prism, and through a triplet achromatic lens, which focuses it into a photomultiplier (PMT), connected to a lock-in amplifier triggered by the chopper. In order to reduce the background during the measurement, the upconverted beam, before reaching the PMT, passes through two UV bandpass filters (Schott UG11) in order to reduce the contribution of the excitation and of the gate to the measurements. The time delay is scanned in order to measure the fluorescence spectrum as a function of excitation-gate delay. Data are collected as single-wavelength traces. The detected wavelength is chosen by rotating the non-linear crystal, thus, determining a certain phase matching angle for the sum frequency process. The calibration of the setup is performed by a simulation which estimates the upconverted wavelength based on the knowledge of the phase matching angle and on the angle between emission and gate beams.

The kinetic trace at 410 nm has been used to estimate the instrumental response function (IRF) of the experiment. The fitting procedure gives back an IRF ≈ 180 fs which corresponds to a time resolution of ≈ 70 fs. The spectral resolution is limited by the acceptance bandwidth of the crystal, and is estimated to be about 13 nm at 550 nm and 26 nm at 700 nm.

Transient Absorption

The femtosecond transient absorption (TA) measurements on the solution of r/p-CQDs excited at 400 nm were based on a 5 kHz Ti:sapphire femtosecond amplifier (Spectra Physics Solstice-Ace) which produces 75 fs pulses peaking at 800 nm (FWHM=30 nm) at 350 µJ/pulse. This beam is split in two parts by a beam splitter (80%/20%) to generate the pump and the probe, respectively.

On the pump arm, the 800 nm beam is frequency-doubled (type I phase-matching) by an ultrathin β–BBO crystal (250 µm) in order to create a 400 nm beam (20% efficiency) which is isolated from the fundamental by a Schott BG40 filter, the beam is chopped at 500 Hz and focused on the sample by a parabolic beam with f=150 mm. The polarization of the pump is controlled by a waveplate. On the second arm, the white light is generated focusing the 800 nm beam in a 1 mm quartz cuvette containing D_2O, generating a broadband pulse extending from 400 to 700 nm. The probe is focused on the sample by the same parabolic mirror used to focus the pump. The pump-probe delay is controlled by a motorized delay stage. The probe and the pump overlap within the sample which continuously flows in a 200 µm thick flow cell upon the action of a peristaltic pump. The flow is regulated in order that every pump pulse hit a fresh portion of the sample.

After the sample, the probe beam is dispersed through a Brewster-angle silica prism and focused on the detector by a lens. The spectral resolution of this configuration is 3 nm. The temporal resolution is about 70 fs. Pump and probe are synchronously with a camera detector system with 1024 pixels (Glaz Linescan-I) with single-shot capability. A typical signal is obtained by averaging 5000 pumped and 5000 unpumped spectra for each delay, and scanning over the pump-probe delay 10-20 times.

The TA measurements with 350 nm excitation have been performed on a setup based on an amplified 1 kHz Ti:sapphire laser system which generates 90 fs pulses centered at 800 nm with 0.8 mJ pulse energy. The beam is split to generate pump and probe. The pump passes through a non-collinear optical parametric amplifier (NOPA) to generate a 700 nm beam. After its generation, the pump pass through a homemade prism-compressor and, then, it is doubled by passing through a nonlinear crystal in order to obtain a 350 nm beam. Then, the excitation beam is chopped at the repetition rate of 500 Hz and focused on the sample. The supercontinuum pulse (350 to 700 nm) is generated by focusing a part of the residual 800 nm beam on a 5 mm-thick CaF_2 crystal. Then it is separated in two identical beams: one (the probe) is overlapped with the pump in the sample, and the other (the reference) is sent through an unpumped volume of the sample to correct for white-light fluctuations on a single shot basis. The detection scheme is the same as for the previous setup. We verified that the results of TA measurements were not concentration dependent. The measurements were carried out under magic angle detection conditions. The data presented in the paper were subjected to standard correction procedures which eliminate the effects of cross-phase modulation (XPM) and group velocity dispersion (GVD).

Results and Discussion

Crystalline graphitic CQDs were synthesized by a top-down approach described in the Experimental section, and in a previous paper by Cayuela et al.[29] We indicate as r-CQDs the dots retrieved immediately after the top-down synthesis, which do not display any steady-state emission. To produce fluorescent CQDs it is necessary, as demonstrated in ref 29, to passivate the surface of the dots with carboxylic moieties. The success of surface passivation has been confirmed by infrared absorption measurements, as shown in Figure 1. In fact, r-CQDs show a single and narrow absorption band at 3460 cm^{-1}, associated with the stretching vibration of isolated -OH groups. After the passivation of the surface by acetone, p-CQDs show a broad band with peaks at 3431 cm^{-1} and 3136 cm^{-1}, associated with hydrogen bonded -OH from carboxyl and hydroxyl groups. Besides, the passivated sample displays peaks associated to -

CH (2995 cm^{-1}) and to -C=O vibrations of carboxyl groups (1710 cm^{-1} and 1644 cm^{-1}). These changes in the FTIR spectrum are the sign of a successful passivation, which introduces a high density of carboxylic and hydroxyl groups on the surface of p-CQDs, with respect to r-CQDs.

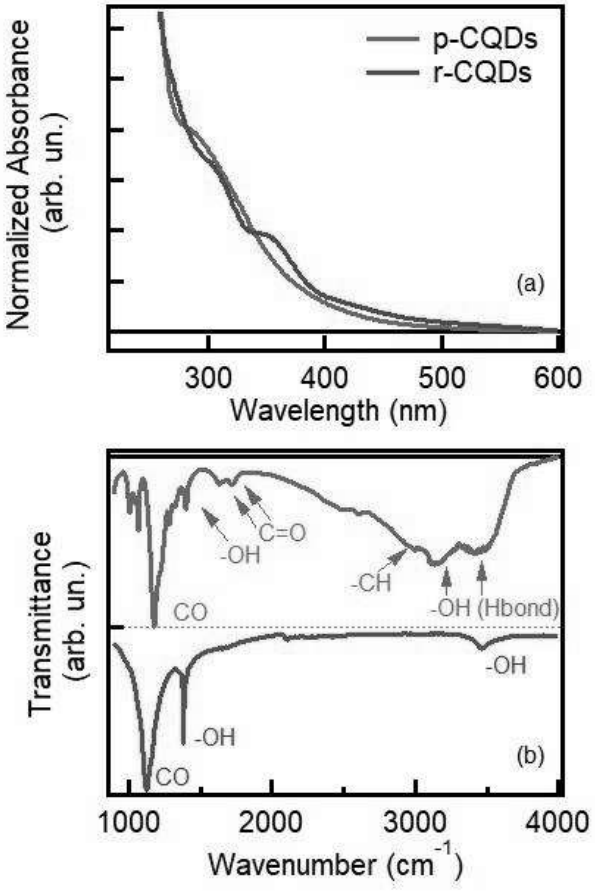

Figure 1: (a) Normalized absorption spectra of aqueous solutions of unpassivated r-CQDs (red curve) and passivated p-CQDs (blue curve). (b) IR spectra of r-CQDs and p-CQDs. Passivation induces a variety of new signals mostly associated to a high density of surface carboxylic and hydroxyl groups.

Beside the different infrared absorption spectrum, the passivated sample shows a slightly different absorption profile (Figure 1a). Most importantly, p-CQDs are found to be luminescent throughout the visible range, displaying an emission (Figure 2) with a Quantum yield (QY) of 4% under excitation at 400 nm. As commonly observed for carbon dots, [7,30-32] the emission in p-CQDs is tunable, meaning that the peak position strongly depends on excitation wavelength (as in Figure 2). Considering that the passivation only changes the surface structure of CQDs, without affecting the core structure, the emission showing up in Figure 2 upon passivation must involve surface states, as already proposed before.[28] The absorption spectra of aqueous solutions of raw and passivated CQDs (r-CQDs and p-CQDs, respectively) are compared in Figure 1a. The two spectra are almost identical below 270 nm, while they display appreciable differences at longer wavelengths. Considering that the core of both r-CQDs and p-CQDs is identical, the absorbance at high energies probably corresponds to electronic transitions related to the graphitic crystalline core. On the contrary, the absorption at long wavelengths is probably related to different surface states hosted by the two samples. In fact, p-CQDs display an extremely broad band (barely visible from the shoulder at 300 nm) which excites the tunable emission displayed in Figure 2, whereas the absorption of r-CQDs shows two more defined bands peaking at 300 nm and 350 nm, which probably correspond to non-emitting surface states, considering that r-CQDs are non-fluorescent.

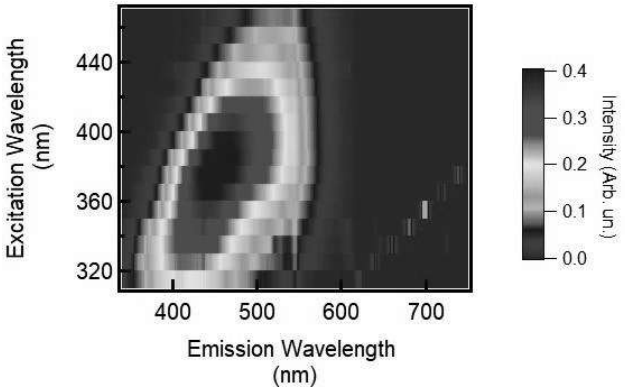

Figure 2: 2D excitation-emission fluorescence maps of p-CQDs. The tilted shape of the 2D map with respect to the axes clearly highlights the tunability of the emission.

To reconstruct the dynamics of the emissive electronic transition from the initial photo-excitation, we performed femtosecond resolved emission measurements by the fluorescence upconversion (FlUC) technique (as described in the SI). Among femtosecond methods, FlUC is particularly suitable to access the very earliest excited-state dynamics after photo-excitation,[33] (time resolution 70 fs) but has been used only rarely so far for carbon dots.[34] Notably, we find that the fluorescence is observable from the very earliest times after photoexcitation, as displayed in Figure 3 (overall emission intensity) and Figure S1 (single-wavelength traces). Thus, the present use of FlUC directly demonstrates that the surface emitting state is directly populated in a very short time, below our experimental time resolution ~ 70 fs. This conclusion contrasts with the existing literature, ruling out the hypothesis of a core-to-surface excitation transfer proposed by other works based on other femtosecond-resolved spectroscopic methods,[16,35] which revealed variable characteristic times for the excitation transfer, ranging from 400 fs to tens of ps. [14,16]

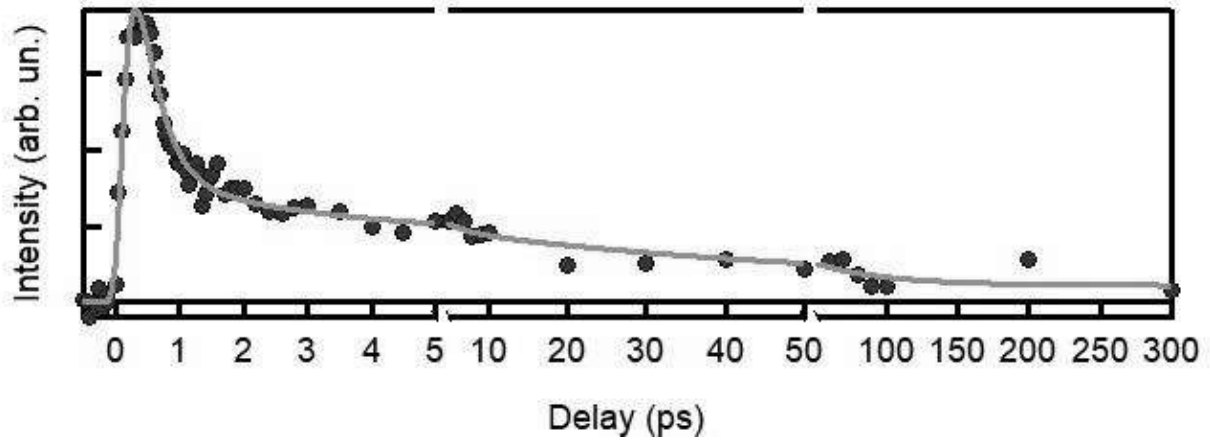

Figure 3: Decay kinetics of the overall emission intensity, as detected in a FLUC experiment, with the least-squares fitting curve. Fluorescence shows up immediately (within 70 fs) after photo-excitation. Thereafter, it partially decays with a multi-exponential kinetics, limiting the overall emission quantum yield. The curve is a best-fitting to the data of a multiexponential decay convoluted with the IRF of the experimental system.

After the instantaneous population of the emissive state, the subsequent fluorescence dynamics (Figure S1) are found to be essentially independent of the emission wavelength, and mostly consist in a strong decaying signal at all wavelengths. A closer inspection of the traces reveals a fast redshift of the signal within 150-200 fs probably due to solvation, as already observed for other types of carbon dots.[7] To increase the signal-to-noise ratio, the kinetics at different wavelengths were averaged and analyzed by least-squares fitting with a multi-exponential function convoluted with the instrumental response function (IRF), as shown in Figure 3. The trace can be reproduced by a rise occurring on a time scale (Table 1) of 0.18 $\pm$ 0.05 ps, and four exponential decays with different timescales and different decay amplitudes: t_1 =0.3 $\pm$ 0.1 ps (86% of decay), t_2 =2.5 $\pm$ 0.1 ps (6% of decay), t_3 =70 $\pm$ 20 ps (6% of decay) and t_4 > 1 ns (2% of decay). Just after photo-excitation, the emission peak is probably closer to the excitation wavelength (400 nm) than our detection (480-650 nm) can reveal. Thus, we attribute the 180 fs rise, as already said, to a solvation-induced redshift of the emitting state, which causes an initial increase of the averaged FlUC signal because the band progressively enters into the detection region from the shorter wavelengths. At later times, the four decays describe the multi-exponential depopulation of the photoexcited state until the formation of a long-lived state. Although in principle the 70 ps component could also be due to a rotational diffusion, transient absorption measurements described in the following allow us to exclude such a mechanism. Consistently with the measured QY, the relative amplitude of the nanosecond-lived component only accounts for 2-4% of the initial population. This agreement leads to another important conclusion: all the non-radiative losses of these CQDs occur in the sub-nanosecond regime, whereas the nanosecond decay is entirely radiative.

In parallel to ultrafast fluorescence measurements, we also carried out pump-probe transient absorption (TA) experiments upon excitation at 400 nm. The signal in Figure 4a can be described as a negative signal around the pump wavelength and a positive signal which involves almost the entire spectral range. In a TA measurement, a negative signal can be a ground state bleaching (GSB), due to the photoinduced depopulation of the ground state, or a stimulated emission (SE) signal, which corresponds to the fluorescence emission band. Considering that the negative signal in our data is peaked around the pump wavelength and that it is relatively narrow, it can be ascribed to a GSB. On the contrary, a positive signal can be only an excited state absorption (ESA) caused by new electronic transitions towards further excited states at higher energy. Considering that a fluorescence is easily visible by FlUC (Figure 3) already at time zero, one would expect to see a SE contribution to the TA spectra around 470 nm. Nevertheless, no SE signal can be identified in the spectra in Figure 4a, probably because it is hidden below the strong and very broad ESA, covering almost the entire spectral range.

Selected kinetic traces from the TA data were analyzed and fitted by a multi-exponential function convoluted with the IRF obtaining almost the same decay times collected in the analysis of FlUC experiment: 0.3 $\pm$ 0.1 ps, 2.6 $\pm$ 0.1 ps, 50 $\pm$ 10 ps and a nanosecond time scale (all the fitting parameters are reported in Table 1 and Table S1). Besides, all the signals detected in TA measurements barely change their shape and, therefore, their dynamics arise only from the same depopulation of a single emitting excited state already detected by FlUC. The earliest component revealed by FlUC (150-200 fs, tentatively ascribed to solvation) is hardly visible in TA due to the lower time resolution or due to the relaxation of the overlapping ESA signal. Noteworthy, the presence of a 50 $\pm$ 10 ps component in the TA measurements at magic angle

condition confirms that the 70 ± 20 ps decay present in the FlUC kinetics describes mainly a depopulation process, as already proposed above.

Table 1. Summary of the characteristic time scales obtained from FlUC and TA experiments.

Time scale	FlUC @400 nm p-CQDs	TA @400 nm p-CQDs	TA @350 nm p-CQDs	TA @350 nm r-CQDs
t_{rise} (ps)	0.18 ± 0.05			
t_1 (ps)	0.3 ± 0.1	0.3 ± 0.1	0.35 ± 0.05	0.5 ± 0.1
t_2 (ps)	2.5 ± 0.1	2.6 ± 0.1	2.2 ± 0.1	1.5 ± 0.1
t_3 (ps)	70 ± 20	50 ± 10	140 ± 10	25 ± 1
t_4 (ps)	> 1 ns	> 1 ns	> 1 ns	> 1 ns

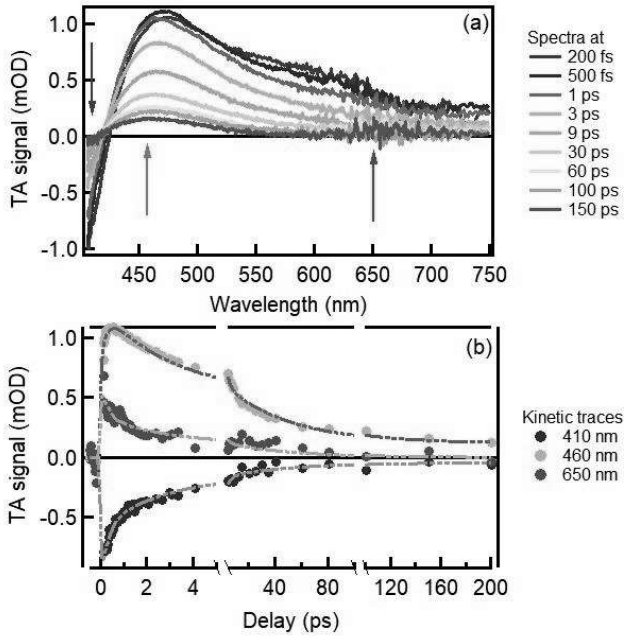

Figure 4: (a) TA spectra of p-CQDs in water excited at 400 nm at various delays after the photoexcitation and (b) Kinetic traces at three representative wavelengths (indicated by the arrows in panel a) fitted by multi-exponential functions convoluted with the IRF of the experimental system.

Fluorescence upconversion and transient absorption measurements allow to describe the system from two complementary points of view. While FlUC singles out the excited-state dynamics by monitoring the spontaneous emission, TA is sensitive to a variety of possible transitions and is capable of probing also the ground-state recovery. Here, both methods concur to picture the photo-cycle of p-CQDs as a very simple one: the direct photoexcitation of the surface emissive state is followed by a strong sub-nanosecond population loss, which explains the low steady-state QY. Similarly to many carbon dots, the fluorescence of these p-CQDs is tunable in the visible range, as displayed in Figure 2. To investigate this characteristic, we performed a second set of pump probe TA measurements, exciting at 350 nm (Figure 5a). We find that both the shape and the dynamics of the TA signal excited at 350 nm are very similar to the one recorded exciting at 400 nm at every delay (Figure S2). As in the previous case, the entire signal can be described as a GSB around the pump wavelength and a broad ESA which covers the entire spectral range. We modelled the dynamics at 350 nm excitation by a multi-exponential fitting of time traces extracted from the TA data. The results are reported in Table 1. Once again, the whole signal undergoes a multi-exponential decay, therefore the excited state undergoes a depopulation after the initial photoexcitation. Comparing the time scales of the two experiments, it is evident that they are almost the same regardless the excitation wavelength. The substantial identity of dynamic evolution and spectral features (except for a rigid shift) upon 400 and 350 nm excitation definitively indicates that the excited chromophore belongs to the same manifold of states having very similar spectroscopic characteristics (shape of the TA signal, ultrafast dynamics, ...). To further emphasize this point, in Figure S2 we compare the spectra after 400 nm and 350 nm excitations. The rigid shift of the TA reflects the tunability of the emission, directly highlighting a redshift of the entire spectrum as a function of excitation wavelength, with only small changes of shape. This behavior was already demonstrated and discussed in a recent work carried out on an entirely different type of carbon dot, [7] and similar results, without interpretations, were reported in another literature work.[36] Therefore, we propose that this behavior is a universal feature of carbon dots. Considering that the visible emission is related to electronic transitions on the surface, [28] the data in Figure S2 suggest that not only the emission, but also the GSB and the ESA are associated with "tunable" surface states which can be described as a manifold covering a continuum of possible energies, associated to dot-to-dot surface structural fluctuations, especially affecting the smallest dots.[7] The small shape variations between the two spectra in Figure S2 are probably due to minor contributions due to core excitation, which probably begins to be significant at 350 nm. Anyway, to further confirm the major involvement of the surface in these dynamics, pump-probe experiments were conducted on solutions of p-CQDs in presence of 80 mM of Cu^{2+} and of Fe^{2+}. The appearance of a new decay component (t = 0.4 ps) in the kinetics (Figure S3), due to the electron transfer from the dot to the ions,[37] confirms that the signal is associated to the depopulation of a state which involves the surface, considering that an electron transfer requires the close contact between the donor and the acceptor. The results in Figure 3, 4 and 5a are fully consistent with a model of p-CQD emission arising from a manifold of surface related states, directly populated by photo-excitation, with no spectroscopic evidence of core states.

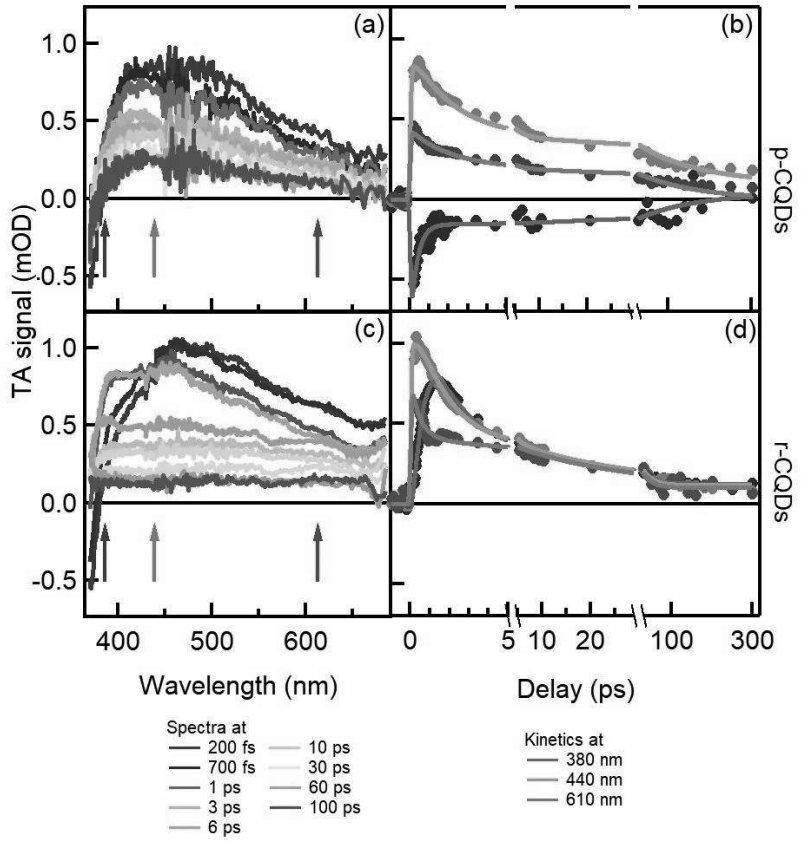

Figure 5: TA spectra of p-CQDs (a) and r-CQDs (c) in water excited at 350 nm at various delays after photoexcitation. TA kinetic traces of p-CQDs (b) and r-CQDs (d) at different wavelengths, indicated by the arrows.

In order to disentangle the role of the core from that of the surface, and to analyze the effect of surface passivation, we repeated the same TA experiment excited at 350 nm also on r-CQDs. Indeed, p-CQDs and r-CQDs have the same core structure and, if core transitions and surface transitions do not interplay with each other, one would expect that the TA signal associated to the core should not change with the passivation. The different results for the two samples are shown in Figure 5, reporting selected TA spectra and kinetic traces obtained from the two samples. The time scales extracted from least-square fitting of the kinetic traces are reported in Table 1. Considering Figure 5 and the time scales reported in Table 1, one can infer that exciting r-CQDs (panels (c) and (d)) produces a signal with a different shape and dynamics. Also in this case, the signal is composed by a GSB around the pump wavelength and a very broad ESA. However, the GSB signal decays completely in few ps, whereas in p-CQDs a GSB signal is still observed even hundreds of ps after photo-excitation (compare spectra at 100 ps in Figure 5a and Figure 5b). After the decay of the GSB, only an ESA remains in r-CQDs. This ESA is very different from that observed in p-CQDs. In fact, the ESA signal of r-CQDs displays a characteristic, flat shape, covering the entire spectral range we probed. We attribute this signal, not observed in p-CQDs, to free electrons in the conduction band of the core. This characteristic ESA resembles the signal which was observed in other TA studies on graphitic dots or graphene quantum dots,[38] suggesting, despite the different synthesis procedure, the involvement of similar electronic core transitions. Focusing now on the dynamics of r-CQDs in the first few picoseconds, in addition to the disappearance of the GSB, one can notice another fast change of the signal in the spectral region below 420 nm. This change can be interpreted as the disappearance, within 1 ps from photo-excitation, of a negative contribution to the TA signal, that is most likely a SE. Such a fast-decaying contribution can be isolated by taking the difference spectrum TA(1 ps) - TA(200 fs) normalized to the amplitude at λ>600 nm: the latter reveals a band peaking at 380 nm, as we show in Figure S4. When compared to the absorption spectrum (see Figure S4) it turns out that this band at 380 nm is almost mirror symmetric to the absorption band peaking at 350 nm. Therefore, the disappearing signal can be interpreted as a very fast-decaying emission, peaking at 380 nm, which is the inverse transition of the 350 nm transition observed in absorption. This result is fully in line with the absence of a steady state emission from r-CQDs. In fact, considering that the absorption spectrum shows some structured bands related to the surface, these should correspond to some electronic transitions which involve the

surface, but which decay through very efficient non-radiative recombination channels, as inferred from the absence of any steady-state emission. Noteworthy, the data collected in r-CQDs lead to the conclusion that the dynamics of core and surface states occur on completely different time scales, with no mutual interaction. On one hand, the dynamics of surface states, revealed by the transient SE signal at 380 nm, only lasts for less than 1 ps. On the other hand, core state dynamics, revealed by the flat ESA, is relatively long lived (hundreds of ps), but does not give rise to any steady state emission. Overall, the dynamics of core and surface states appear to be completely independent from each other.

Despite the core of p-CQDs and r-CQDs is the same, the dynamics of p-CQDs are overwhelmingly dominated by surface states, whereas only in r-CQDs core and surface dynamics can be observed both. In fact, the surface states introduced in p-CQDs by passivation are so strongly absorbing that the contribution of core states becomes practically negligible in all the observed dynamics. On the contrary, core dynamics can be easily revealed in r-CQDs because a sizeable fraction of optical absorption is due to core transitions, combined with the fact that core states are comparatively longer lived (100 ps) than photo-excited surface states (1 ps).

The full disentanglement of core- and surface-state dynamics, and the lack of any interaction between the two, demonstrated here by means of femtosecond optical methods, provides a new viewpoint on the photo-physics of CQDs which we consider an especially relevant conclusion of this work. Further studies may help to find out to what extent these conclusions can be generalized to other types of carbon nanodots fabricated or passivated by entirely different physico-chemical routes.

Conclusions

The synergy of traditional steady-state OA and fluorescence experiments with femtosecond-resolved fluorescence and pump-probe spectroscopy excited at variable wavelengths allowed to fully disentangle the contributions of core and surface structures to the complex photo-excited dynamics of raw and passivated graphitic CQDs. Summarizing the obtained results, it is possible to draw several conclusions on the photo-excitation and de-activation mechanisms of the two types of nanoparticles and, therefore, on the critical effects of surface passivation on carbon dots.

Unpassivated r-CQDs display two parallel and independent photo-excitation channels, associated to the surface and the core structures, respectively. Excited core states show up as an extremely broad excited-state absorption signal, and slowly depopulate (hundreds of ps) via band to band recombination. In contrast, surface dynamics are characterized by a fluorescent state which suffers an extremely efficient (<1 ps) non-radiative channel. Noteworthy, the observation of this emission clearly demonstrates, for the first time, that even the surface of raw dots hosts electronic states which would be theoretically capable of fluorescence, but they recombine too fast to be observable in a steady-state experiment.

Once the surface is passivated, the situation becomes quite different, as demonstrated by various substantial changes of the OA and fluorescence spectra, both in steady-state and in the femtosecond regime. In fact, passivation introduces an entirely new manifold of surface-localized electronic states, responsible of a long-lived fluorescence tunable across the visible range. Moreover, ultrafast experiments allow picturing the photo-excitation of passivated p-CQDs as a direct population of the surface emissive state, ruling out any crosstalk with core states. We also find the emissive surface state to undergo partial sub-nanosecond depopulation, and estimate the characteristic time scale of the latter, which turns out to be the main limiting factor of p-CQDs fluorescence efficiency.

Conflicts of interest

There are no conflicts to declare.

Acknowledgements

A. S., M. C. and F. M. thank the Laboratory "Roberto Boscaino" of Advanced Materials (LaBAM) group (www.unipa.it/lamp) at University of Palermo for support and stimulating discussions. This research was supported by the Spanish Ministry of Innovation and Science for the funding project ref. CTQ2017-83175R. M. L. S. expresses her gratitude for the funding project (ref SBPLY/17/180501/000333) to the European Commission and to the JJCC Castilla-La Mancha. A. S., M. G., and A. C. acknowledge the Swiss NSF via the NCCR MUST and the project n. 200021172696.

Notes and references

1 Y. Sun, B. Zhou, Y. Lin, W. Wang, K. A. S. Fernando, P. Pathak, M. J. Meziani, B. A. Harruff, X. Wang, H. Wang, P. G. Luo, H. Yang, M. E. Kose, B. Chen, L. M. Veca and S. Xie, *J. Amer. Chem. Soc.*, 2006, **128**, 7756–7757.

2 X. Wang, S.-T. Wang, F. Lu, M. J. Meziani, L. Tian, K. W. Sun, M. A. Bloodgood and Y.-P. Sun, *Angew. Chem. Int. Ed*, 2010, **122**, 5438–5442.

3 J. Hou, W. Wang, T. Zhou, B. Wang, H. Li and L. Ding, *Nanoscale*, 2016, **8**, 11185–11193.

4 A. Sciortino, A. Cannizzo and F. Messina, *C*, 2018, **4**, 67.

5 A. Cayuela, M. L. Soriano, C. Carrillo-Carrion and M. Valcarcel, *Chem. Commun.*, 2016, **52**, 1311–1326.

6 S.-T. Yang, L. Cao, P. G. Luo, F. Lu, X. Wang, H. Wang, M. J. Meziani, Y. Liu, G. Qi and Y.-P. Sun, *J. Amer. Chem. Soc.*, 2009, **131**, 11308–11309.

7 A. Sciortino, M. Gazzetto, G. Buscarino, R. Popescu, R. Schneider, G. Giammona, D. Gerthsen, E. J. Rohwer, N. Mauro, T. Feurer, A. Cannizzo and F. Messina, *Nanoscale*, 2018, **10**, 15317–15323.

8 H. Li, X. He, Z. Kang, H. Huang, Y. Liu, J. Liu, S. Lian, C. H. A. Tsang, X. Yang and S.-T. Lee, *Angew. Chem. Int. Ed.*, 2010, 4430–4434.
9 P. Yu, X. Wen, Y.-R. Toh and J. Tang, *J. Phys. Chem. C*, 2012, **116**, 25552–25557.
10 L. Shi, J. H. Yang, H. B. Zeng, Y. M. Chen, S. C. Yang, C. Wu, H. Zeng, O. Yoshihito and Q. Zhang, *Nanoscale*, 2016**, 8**, 14374–14378.
11 W. Wang, B. Wang, H. Embrechts, C. Damm, A. Cadranel, V. Strauss, M. Distaso, V. Hinterberger, D. M. Guldi and W. Peukert, *RSC Adv.*, 2017, **7**, 24771–24780.
12 A. Sciortino, E. Marino, B. v. Dam, P. Schall, M. Cannas and F. Messina, *J. Phys. Chem. Lett*., 2016, **7**, 3419–3423.
13 L. Wang, S.-J. Zhu, H.-Y. Wang, S.-N. Qu, Y.-L. Zhang, J.-H. Zhang, Q.-D. Chen, H.-L. Xu, W. Han, B. Yang and H.-B. Sun, *ACS Nano*, 2014, **8**, 2541–2547.
14 L. Sui, W. Jin, S. Li, D. Liu, Y. Jiang, A. Chen, H. Liu, Y. Shi, D. Ding and M. Jin, *Phys. Chem. Chem. Phys.*, 2016, 3838–3845.
15 S. Lu, G. Xiao, L. Sui, T. Feng, X. Yong, S. Zhu, B. Li, Z. Liu, B. Zou, M. Jin, J. S. Tse, H. Yan and B. Yang, *Ang. Chem. Int. Ed.*, 2017, **56**, 6187–6191.
16 V. Strauss, A. Kahnt, E. M. Zolnhofer, K. Meyer, H. Maid, C. Placht, W. Bauer, T. J. Nacken, W. Peukert, S. H. Etschel, M. Halik and D. M. Guldi, *Adv. Func. Mater.*, 2016, **26**, 7975–7985.
17 S. Zhu, J. Zhang, X. Liu, B. Li, X. Wang, S. Tang, Q. Meng, Y. Li, C. Shi, R. Hu and B. Yang, *RSC Adv.*, 2012, **2**, 2717–2720.
18 A. B. Bourlinos, A. Stassinopoulos, D. Anglos, R. Zboril, M. Karakassides and E. P. Giannelis, *Small*, 2008, 455–458.
19 L. Sciortino, A. Sciortino, R. Popescu, R. Schneider, D. Gerthsen, S. Agnello, M. Cannas and F. Messina, *J. Phys. Chem. C*, 2018, **122**, 19897–19903.
20 M. J. Krysmann, A. Kelarakis, P. Dallas and E. P. Giannelis, *J. Amer. Chem. Soc*., 2012**, 134**, 747–750.
21 X. Hu, L. Cheng, N. Wang, L. Sun, W. Wang and W. Liu, *RSC Adv.*, 2014, **4**, 18818–18826.
22 S. W. Chung, E. A. Guliants, C. E. Bunker, D. W. Hammerstroem, Y. Deng, M. A. Burgers, P. A. Jelliss and S. W. Buckner, *Langmuir*, 2009, **25**, 8883–8887.
23 E. Marino, T. E. Kodger, G. H. Wegdam and P. Schall, *Adv. Mater*, 2018, **30**, 1803433.
24 H. Zhu, X. Wang, Y. Li, Z. Wang, F. Yang and X. Yang, *Chem. Commun.*, 2009, 5118–5120.
25 A. Cayuela, M. L. Soriano and M. Valcarcel, *Anal. Chim. Acta*, 2015, **872**, 70–76.
26 A. Cayuela, M. L. Soriano, M. C. Carrion and M. Valcarcel, *Anal. Chim. Acta*, 2014, **820**, 133–138.
27 X. Li, S. Zhang, S. A. Kulinich, Y. Liu and H. Zeng, *Sci. Rep.*, 2014**, 4**, 4976.
28 A. Sciortino, A. Cayuela, M. L. Soriano, F. M. Gelardi, M. Cannas, M. Valcarcel and F. Messina, *Phys. Chem. Chem. Phys.*, 2017, **19**, 22670–22677.
29 A. Cayuela, M. L. Soriano and M. Valcarcel, *Anal. Chim. Acta*, 2013, **804**, 246–251.
30 H. Nie, M. Li, Q. Li, S. Liang, Y. Tan, L. Sheng, W. Shi and S. X.-A. Zhang, *Chem. Mater.*, 2014, **26**, 3104–3112.
31 O. Kozak, K. K. Datta, M. Greplova, V. Ranc, J. Kaslik and R. Zboril, *J. Phys. Chem. C*, 2013, **117**, 24991–24996.
32 L. Guo, J. Ge, W. Liu, G. Niu, Q. Jia, H. Wang and P. Wang, *Nanoscale*, 2016, **8**, 729–734.
33 F. Messina, E. Pomarico, M. Silatani, E. Baranoff and M. Chergui, *J. Phys. Chem. Lett.*, 2015, **6**, 4475–4480.
34 L. Wang, S.-J. Zhu, H.-Y. Wang, Y.-F. Wang, Y.-W. Hao, J.-H. Zhang, Q.-D. Chen, Y.-L. Zhang, W. Han, B. Yang and H.-B. Sun, *Adv. Opt. Mater.*, 2013, **1**, 264–271.
35 S. Lu, L. Sui, J. Liu, S. Zhu, A. Chen, M. Jin and B. Yang, *Adv. Mater.*, 2017, **29**, 1603443.
36 S. Zhu, J. Shao, Y. Song, X. Zhao, J. Du, L. Wang, H. Wang, K. Zhang, J. Zhang and B. Yang, *Nanoscale*, 2015, **7**, 7927–7933.
37 A. Sciortino, A. Madonia, M. Gazzetto, L. Sciortino, E. J. Rohwer, T. Feurer, F. M. Gelardi, M. Cannas, A. Cannizzo and F. Messina, *Nanoscale*, 2017, **9**, 11902–11911.
38 W. Kwon, Y.-H. Kim, J.-H. Kim, T. Lee, S. Do, Y. Park, M. S. Jeong, T.-W. Lee and S.-W. Rhee, *Sci. Rep.*, 2016, **6**, 24205.